Article

A Study on the Ultimate Strength and Failure Mode of Stiffened Panels

Qi Zhang [1], Hongqi Yang [1,*], Shuang Wu [1], Wenbo Cheng [1], Yuanhua Liang [2] and Yi Huang [1]

1   School of Naval Architecture, Dalian University of Technology, Dalian 116024, China
2   Offshore Engineering Technology Center CCS, Tianjin 300457, China
*   Correspondence: yanghq@dlut.edu.cn

Abstract: Different buckling failure modes of stiffened panels will result in differences in ultimate strengths. In this study, the benchmark model of the bottom of bulk carrier with appropriate initial imperfections, boundary conditions and mesh size are selected for a series of non-linear FE analyses. A failure mode discrimination method considering the change rule of ultimate strength and the stress and strain distribution of stiffened plates in ultimate limit state is proposed, and then the boundary function of the failure modes composed of four key parameters, λ, β, h_w/t_w, λ_e, is established. Based on this boundary function, the rapid identification of failure modes and the classification of ultimate strength under different failure modes can be realized. Furthermore, the ultimate strength formulas of stiffened panels for different failure modes are obtained by data analysis from many nonlinear finite element analyses.

Keywords: stiffened panel; ultimate strength; failure mode

1. Introduction

Stiffened panels composed of plating and stiffeners are widely used in hull structures because of their light weight, high stiffness and high material utilization rate. However, in offshore practice, the collapse of stiffened panels is fairly common, making it of great significance to establish an accurate and effective method for evaluating the ultimate strength of stiffened panels.

Numerous studies have been completed to establish empirical formulas for predicting the ultimate strength of stiffened panels. Paik [1,2] derived an empirical formula for the ultimate strength of stiffened panels under uniaxial compression based on compression test data of stiffened panels of different sizes, and the empirical formula contains two parameters: the plate slenderness and column slenderness. Khedmati [3] proposed a formula for the prediction of the ultimate strength of aluminum stiffened panels under the combination of biaxial compression and lateral pressure. T-stiffeners and a flat bar were considered and lateral pressure was characterized by water head. Zhang [4] conducted numerical simulation and experimental verification of the ultimate strength of stiffened panels under uniaxial compression and proposed a more concise formula. Faulkner [5] analyzed the post-buckling capacity of a plate and the supporting effect of the stiffeners and proposed a formula for the average stress of the overall cross-section of stiffened panels. To consider the influence of the stiffener type, Xu [6] added several terms to the relevant parameters of Paik's formula, proposed an empirical formula shape with 10 coefficients, and carried out data fitting and experimental verification.

The numerical simulation method is widely used in the study of the ultimate strength of stiffened panels. In the process of numerical simulation, factors such as structural forms, model range, and initial imperfections are fully considered, which provides a valuable reference. However, as a thin-walled composite structure, the stiffened panel will collapse in various modes due to the difference in stiffness between the plating and the stiffener,

which makes it necessary to consider failure modes when studying the ultimate behaviour of stiffened panels.

After investigating the effects of factors such as the shape and size of an initial imperfection, the magnitude and direction of the residual stress, and the cross-sectional area ratio between the plating and stiffener on the axial load capacity and failure mode of stiffened panels, Grondin [7] found that the relative size of the torsional stiffness of the stiffener and the bending stiffness of the plate are the key factors that determine the occurrence of stiffener tripping and local plate buckling. Through investigations, model tests and numerical simulations, Zhang [4] proved that the failure mode of stiffened panels under axial compression manifested as coupled bending and torsion failure, which are mainly determined by beam–column behaviours. Ozgur [8] compared the ultimate strength of stiffened panels obtained using ABAQUS and PULS, and found that the greatest deviation usually occurs in areas where the failure modes are inconsistent. The ISSC [9] Ultimate Strength Committee initiated a benchmark study on the ultimate state analysis of stiffened plate structures subjected to uniaxial compression loads. The finite element results of 17 groups, which were compared with each other and with the experimental results. It was found that the failure mode of stiffened panel was not precisely predicted, which may be due to the inaccurate modeling of residual stress. The Committee recommends that more research on failure modes needs to be carried out to define and predict structural failure.

According to the research of Paik [10], the failure modes of stiffened panels subject to axial compression can be divided into six types, as shown in Figure 1: overall buckling (mode I), local plate buckling (mode II), beam–column buckling (mode III), stiffener web buckling (mode IV), stiffener tripping (mode V) and overall yielding (mode VI). Among them, local plate buckling (mode II), beam–column buckling (mode III), stiffener web buckling (mode IV), and stiffener tripping (mode V) are more common in offshore practice.
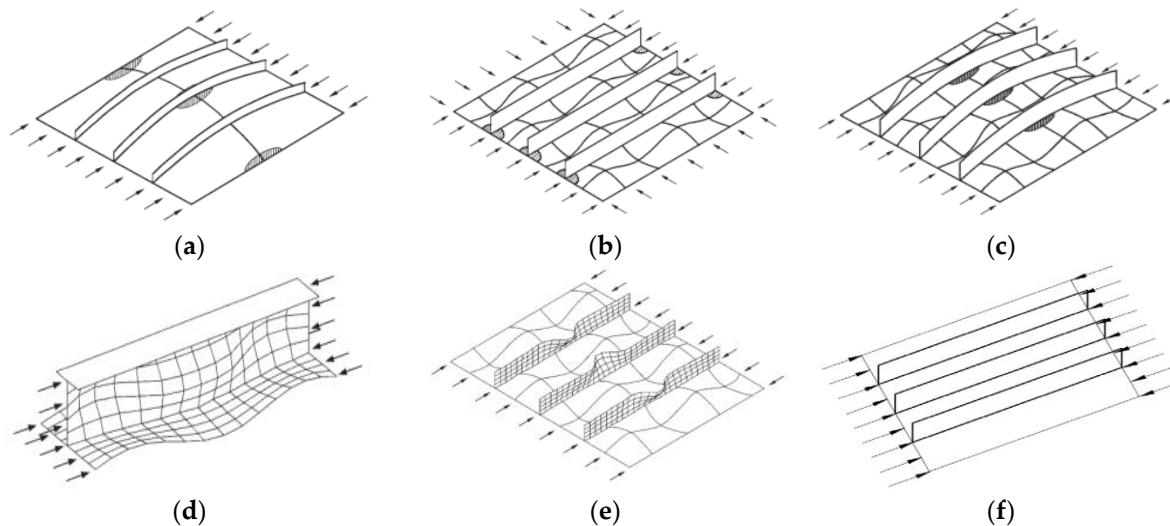
Figure 1. Six failure modes of stiffened panels. (**a**) I: Overall buckling; (**b**) II: local plate buckling; (**c**) III: beam–column buckling; (**d**) IV: stiffener web buckling; (**e**) V: stiffener tripping; (**f**) VI: overall yielding.

Mode II: The relatively weak plating severely deforms, and the stress concentrates at the corners of the plating between stiffeners.

Mode III: The principle of beam–column buckling is similar to that of the bending buckling of bars. The plating and stiffener are considered an entity due to their similar stiffness, and the collapse occurs mid-span. Without a violent deformation process, beam–column buckling is regarded as a relatively safe failure mode. A slight change in the size of the stiffened panel will not lead to a drastic change in the ultimate strength.

Mode IV: Stiffener panels are prone to collapse in this mode when the web of the stiffener has a large height-to-thickness ratio. As the main stiffened component, the stiffener

bears the maximum load of the structure. However, the lack of stiffness often results in buckling on the web, and consequently lead to a sharp increase in the collapse probability of stiffened panel.

Mode V: Due to the small torsional stiffness, the stiffener twists around the intersection line of the stiffeners and the plating under axial compressive. Unlike beam–column buckling, the stiffened panel collapses sharply in a dangerous mode without the support of the stiffener. A slight reduction in the size of the stiffened panel may lead to a sharp decrease in the ultimate strength.

In summary, a great deal of work has been conducted on the formula for ultimate strength and the identification of failure modes of stiffened panels, which can provide us with valuable references. Nevertheless, a single line shape formula for stiffened panels containing only two parameters, λ and β, fails to disclose the effect of failure modes, and there are still deficiencies in the study of the key parameters, evolution and boundaries of different failure modes.

From the above-mentioned situation, a study based on the failure modes is conducted. A new method of failure mode identification based on the variation trend of the ultimate strength and stress distribution in the ultimate limit state is proposed. Based on this method, the boundary between different failure modes is determined and a four-parameter ultimate strength formula applicable to different failure modes is proposed.

2. Modelling for FE Analysis

The finite element solver ANSYS was used for the analysis of ultimate limit state capacity of stiffened panel. The modeling of the stiffened panel, the application of the initial deformation and the post-processing work were all realized by ANSYS parametric design language (APDL).

In this paper, the advanced buckling analysis method recommended by the International Association of Classification Societies (IACS), which is based on nonlinear analysis techniques, was used to study the ultimate strength of stiffened panels. Nonlinear buckling analysis is a static analysis method based on factors such as elastic–plastic material properties, large deformation and initial imperfections. The model of an ideal elastic–plastic material was adopted and the effect of strain-hardening was ignored. To track the post-buckling process of the structure, the Riks method was used to solve the complex load and displacement paths in the post-buckling stage of the structure by introducing a load factor to link the load and displacement.

2.1. Geometric and Material Properties

The ultimate strength of stiffened panels is related to the material parameters, geometric dimensions, initial defects, and load conditions. With reference to the benchmark model Panel A in ISSC2012 [11], the ultimate strength of stiffened panels under uniaxial longitudinal compression was studied. The structure and size of the stiffened panel are shown in Figure 2. The stiffened panel was made of hull steel, and the material was assumed to be uniform, continuous, isotropic and ideal elastoplastic, satisfying the Von Mises yield criterion. The relevant parameters are shown in Table 1. The Shell181 element was used to establish the stiffened panel model, which has four nodes; each node contains six degrees of freedom. This element can be applied to linear, large rotation or large strain analysis. Allowing for both geometric and material nonlinearities, Shell181 is well-suited to simulating thin and medium-thickness shells. In the element domain, both full and reduced integration schemes are supported. For stiffened panels, the ideal choice is to use a reduced integration for the plating and a full integration for the stiffeners.
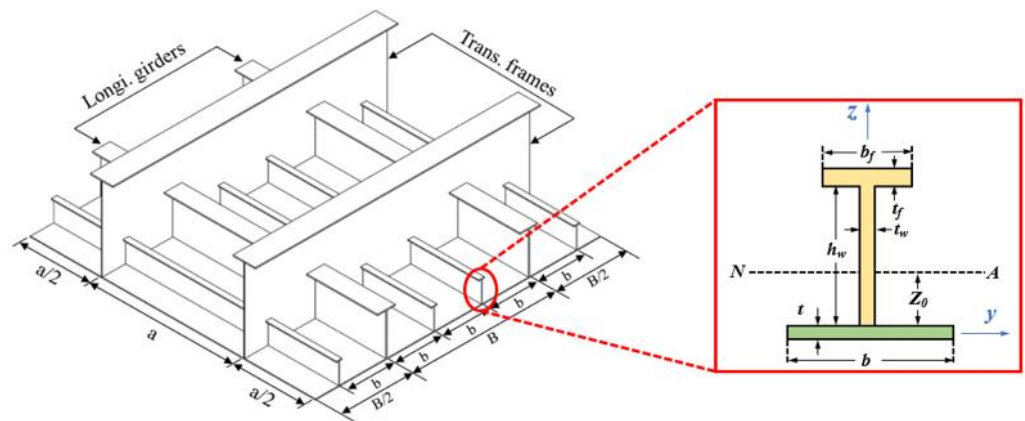
Figure 2. Benchmark model of the bulk carrier bottom panel.

Table 1. Material and geometric parameters of stiffened panels.

Physical Quantity/Units	Symbol	Value
Plate length/mm	a	2550
Plate width/mm	b	850
Plate thickness/mm	t	9.5, 11, 13, 16, 22, 33
Stiffener size 1/mm	$h_w \times b_f \times t_w/t_f$	$138 \times 90 \times 9/12$
Stiffener size 2/mm	$h_w \times b_f \times t_w/t_f$	$235 \times 90 \times 10/15$
Stiffener size 3/mm	$h_w \times b_f \times t_w/t_f$	$383 \times 100 \times 12/17$
Stiffener size 4/mm	$h_w \times b_f \times t_w/t_f$	$580 \times 150 \times 15/20$
Elastic modulus/MPa	E	2.058×10^5
Yield stress/MPa	σ_s	313.6
Poisson's ratio	μ	0.3

2.2. Initial Imperfections

An initial imperfection contains initial deformation and residual stress, which often leads to a reduction in the ultimate strength regarding the analysis of problems involving structural instabilities. Therefore, it is necessary for the finite element model to reasonably include initial imperfections.

The residual stress distribution of each part of a stiffened panel differs, and the stress amplitude is greatly affected by temperature. At the same time, a hull structure subjected to a cyclic wave force undergoes residual stress redistribution and relaxation. Therefore, in the numerical calculation of stiffened panels, the residual stress is usually ignored.

Initial deformation can be directly measured by scanning equipment. When the measurement is difficult or the data reliability is poor, a modal analysis method can be adopted to obtain the lowest buckling mode and the initial deformation. This paper refers to the ISSC to impose the buckling initial deformation on the stiffened panels. The initial deformation expressions for local plate buckling w_{opl}, beam–column buckling w_{oc}, and stiffener tripping w_{os} are as follows:

$$w_{opl} = A_0 \sin(m\pi x/a) \sin(\pi y/b)$$

$$w_{oc} = B_0 \sin(\pi x/a) \sin(\pi y/B)$$

$$w_{os} = C_0(z/h_w) \sin(\pi x/a)$$

where $A_0 = 0.1\beta^2 t$ (moderate deformation), buckling periodic waves $m = 3$ (the smallest integer that satisfies $a/b \leq \sqrt{m(m+1)}$), $B_0 = 0.0015a$, $C_0 = 0.0015a$, and the plate width between the longitudinal girders $B = 3b$.

The final initial deformations are obtained by superimposing these three initial deformations and created by an APDL program according to the coordinates calculated by the above equation.

2.3. Boundary Conditions

The boundary conditions were set is based on Xu [12]. Taking a stiffened panel with a thickness of 16 mm and stiffeners of size 3 as an example, Figures 3 and 4 show the size and stress distribution in the ultimate state of the single-stiffener model, symmetrical model (half model in the longitudinal direction) and periodic model (Panel A). The ultimate strength of these three models is shown in Table 2.
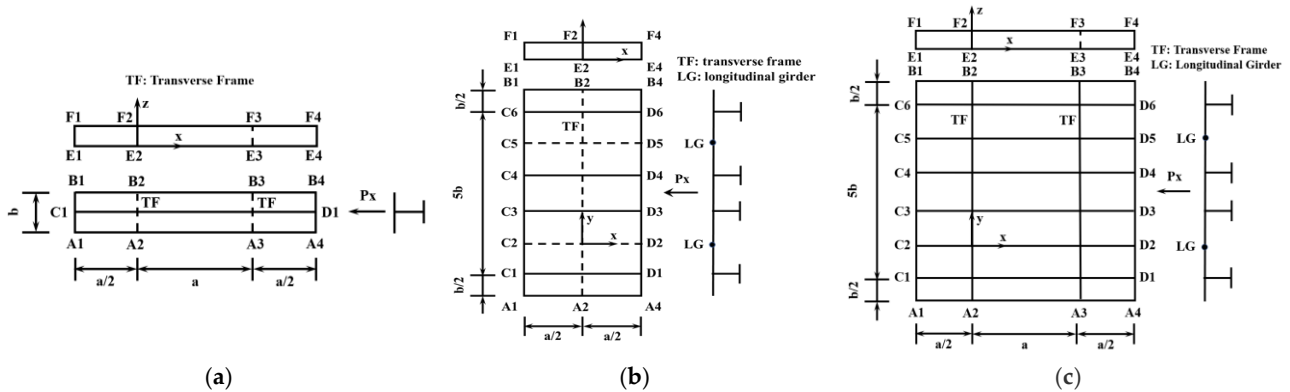

(a)　　　　　　　　(b)　　　　　　　　(c)

Figure 3. Boundary constraints of the stiffened panels. (**a**) Single-stiffener; (**b**) symmetrical; (**c**) periodic.
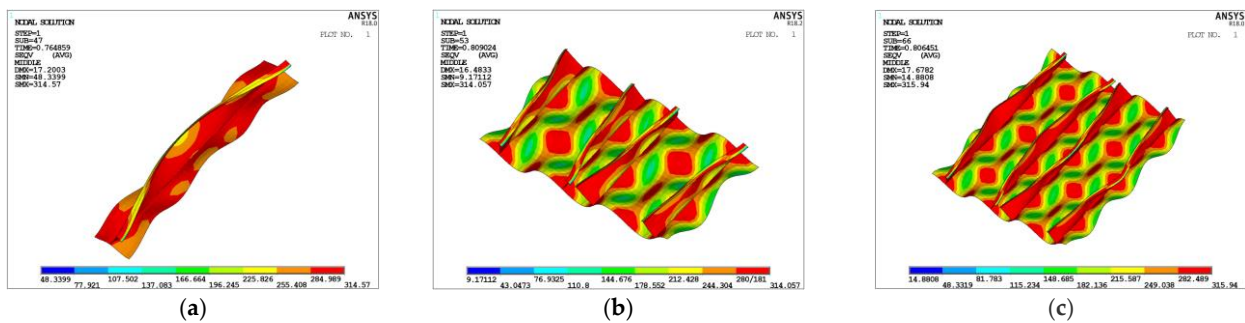

(a)　　　　　　　　(b)　　　　　　　　(c)

Figure 4. Comparison of equivalent stress results under three boundary conditions. (**a**) Single-stiffener; (**b**) symmetrical; (**c**) periodic.

Table 2. Ultimate strength results for different model ranges.

Model Range	Single-Stiffener	Symmetrical	Periodic
Ultimate strength/MPa	283.544	237.979	237.973

The accuracy of the ultimate strength of the single-stiffener model is low, while the results of the symmetrical model and the periodic model are essentially the same. The boundary conditions of the two models are shown in Tables 3 and 4. 0, and indicate constraint. To observe the failure modes comprehensively, periodic boundary conditions are selected.

Table 3. Periodic boundary conditions.

| |
|---|
| $A_2 - B_2$, $A_3 - B_3$: $u_z = 0$, $\theta_x = 0$ |
| $A_1 - A_4$: $u_y = 0$, $\theta_x = 0$, $\theta_z = 0$ |
| $B_1 - B_4$: $u_y = C_{dy1}$(Coupling in the y direction), $\theta_x = 0$, $\theta_z = 0$ |
| $A_1 - B_1$: $u_x = 0$, $\theta_y = 0$, $\theta_z = 0$ |
| $A_4 - B_4$: $u_x = C_{dx1}$(Coupling in the x direction), $\theta_y = 0$, $\theta_z = 0$ |
| $E_2 - F_2$, $E_3 - F_3$: $u_y = C_{dy2}$(Coupling at each web), $\theta_x = 0$ |
| $E_1 - F_1$ at C_1, C_3, C_4 and C_6 (including flange) : $u_x = 0$, $\theta_y = 0$, $\theta_z = 0$ |
| $E_4 - F_4$ at D_1, D_3, D_4 and D_6 (including flange) : $u_x = C_{dx2}$, $\theta_y = 0$, $\theta_z = 0$ |
| $C_2 - D_2$, $C_5 - D_5$: $u_z = 0$, $\theta_y = 0$ |

Table 4. Symmetric boundary conditions.

$A_2 - B_2$: $u_z = 0$, $\theta_x = 0$
$A_1 - A_4$: $u_y = 0$, $\theta_x = 0$, $\theta_z = 0$
$B_1 - B_4$: $u_y = C_{dy}$(Coupling in the y direction), $\theta_x = 0$, $\theta_z = 0$
$A_1 - B_1$: $u_x = 0$, $\theta_y = 0$, $\theta_z = 0$
$A_4 - B_4$: $u_x = C_{dx}$(Coupling in the x direction), $\theta_y = 0$, $\theta_z = 0$
$E_2 - F_2$: $u_y = C'_{dy}$(Coupling at each web), $\theta_x = 0$
$E_1 - F_1$ at C_1, C_3, C_4 and C_6 (including flange) : $u_x = 0$, $\theta_y = 0$, $\theta_z = 0$
$E_4 - F_4$ at D_1, D_3, D_4 and D_6 (including flange) : $u_x = C'_{dx}$, $\theta_y = 0$, $\theta_z = 0$
$C_2 - D_2$, $C_5 - D_5$: $u_z = 0$, $\theta_y = 0$

2.4. Mesh Size

The mesh size determines the total number of elements. To find a balance between computational expense and accuracy, a stiffened panel with a plate thickness of 16 mm and stiffeners of size 3 was used for convergence verification of the mesh size. The number of elements with plating, flange and web was set to N_p, N_f, N_w respectively.

Take the number of elements with plating as an example. Four mesh sizes of 213.50 mm (N_p = 12), 106.25 mm (N_p = 24), 53.125 mm (N_p = 48) and 26.563 mm (N_p = 96) were selected for tentative calculation. As Figure 5a shows, when the mesh size is less than 106.25 mm (N_p = 24), the reduction in the mesh brings little benefit in terms of accuracy. The difference in ultimate strength between 106.25 mm (N_p = 24) and 53.125 mm (N_p = 48) mesh sizes is only 0.6%. The mesh size of 106.25 mm (N_p = 24) can be considered to meet the convergence requirements, so the 106.25 mm (N_p = 24) mesh size was set for calculation. Similarly, the numbers of elements of the stiffener flange and web were set as 4 and 5, respectively, as shown in Figure 6.
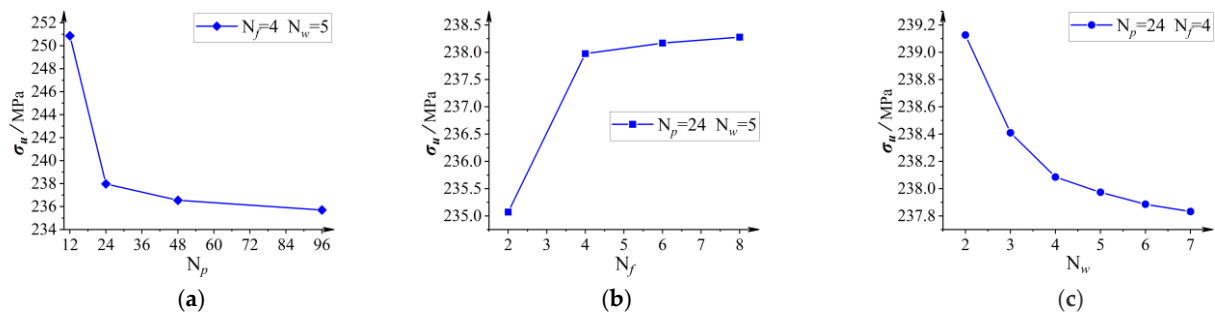
Figure 5. Ultimate strength with different element numbers. (**a**) Element number of the plating; (**b**) Element number of the flange; (**c**) Element number of the web.
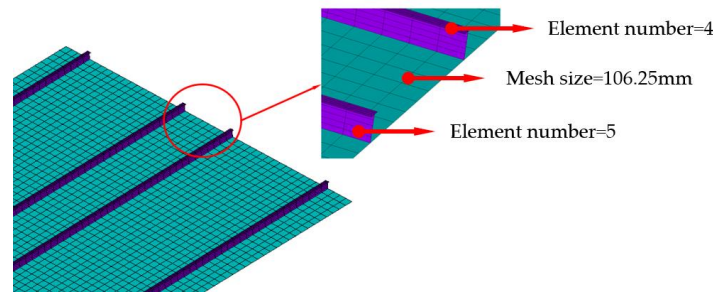
Figure 6. Mesh of stiffened panels.

2.5. Model Verification

In this paper, several stiffened panels with different plating thicknesses and stiffener sizes were selected for the ultimate strength calculation, and the calculation results are compared with the results in the related literature in Table 5. Under the same conditions, such as the same size stiffener and same initial imperfections, the error in the results is within ±3%, which means that the results are within a reasonable range and the model is sufficiently accurate.

Table 5. Comparison of the calculation results of the ultimate strength of the stiffened panels.

Source of Data	Thickness of the Plating (mm)	Size of the Stiffener	σ_u/σ_s from the Literature	σ_u/σ_s from This Paper	Error
Frieze P A, Abbattista M, Vallascas M, et al. [13] (MSC/MARC)	9.5	size 1	0.595	0.590	−0.8%
		size 2	0.641	0.629	−1.9%
		size 3	0.659	0.653	−0.9%
		size 4	0.680	0.672	−1.2%
ISSC2012 [11] (ANSYS(ULG))	9.5	size 3	0.635	0.653	2.8%
	11		0.653	0.672	2.9%
	13		0.688	0.702	2.0%
	16		0.747	0.759	1.6%
	22		0.865	0.883	2.1%
	33		0.964	0.985	2.2%

3. Study on Beam–Column Buckling and Local Plate Buckling

3.1. Theoretical Formula

The principle of beam–column buckling is similar to the bending buckling of bars. Solving the deflection curve differential equation leads to the ideal elastic buckling critical stress formula:

$$\sigma_E/\sigma_s = 1/\lambda^2 \tag{1}$$

where $\lambda = [a/(\pi r)]\sqrt{\sigma_s/E}$ represents the slenderness of the stiffener, $r = \sqrt{I/A}$ represents the radius of inertia of the section, I represents the moment of inertia of the section, and $A = h_f * t_f + h_w * t_w$ is the area of the cross-section. The elastic buckling stress and yield stress of the panels are denoted as σ_E and σ_s, respectively. σ_E and λ are negatively correlated, and λ can be selected as the mechanical parameter for evaluating beam–column buckling.

The principle of local plate buckling is based on the post-buckling performance of the plate. When the plate reaches the ultimate strength, the critical stress formula [14] is as follows:

$$\sigma_u/\sigma_s = \pi/(\beta\sqrt{3(1-\mu^2)}) = 1.9/\beta \tag{2}$$

where $\beta = (b/t)\sqrt{\sigma_s/E}$, σ_u represents the ultimate strength of the stiffened panel, which is negatively correlated with β, and β can be selected as the mechanical parameter for evaluating local plate buckling.

3.2. Identification of Beam–Column Buckling and Local Plate Buckling

Taking size 1 and size 2 as examples, the equivalent stress plots of typical beam–column buckling and local plate buckling are shown in Figures 7 and 8, respectively.
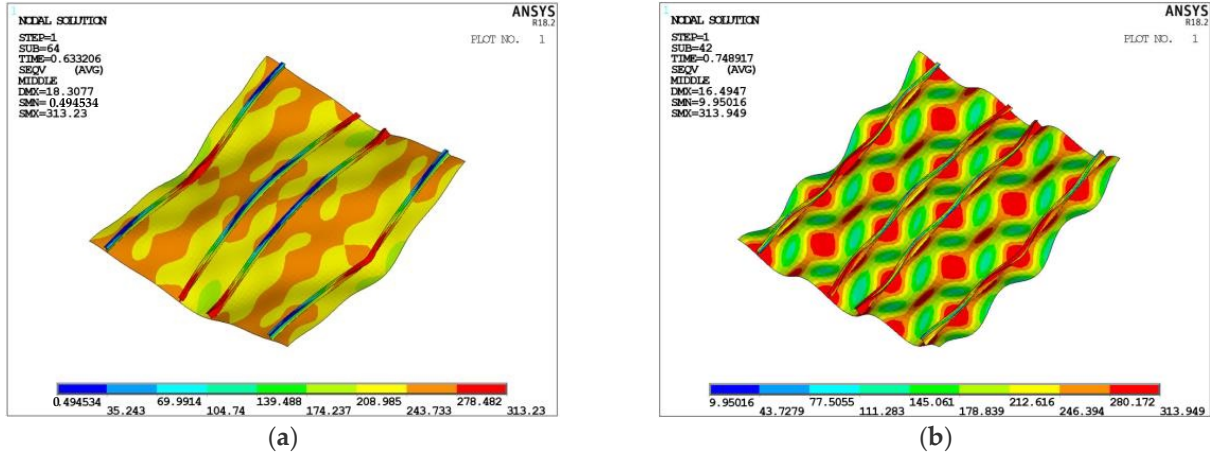

Figure 7. Beam–column buckling (**a**) and local plate buckling (**b**) (size 1).
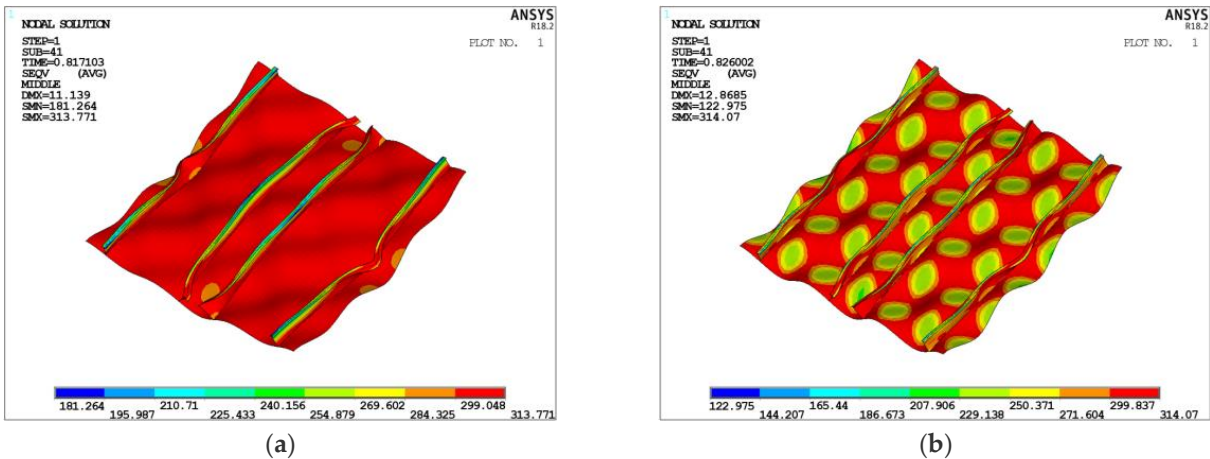

Figure 8. Beam–column buckling (**a**) and local plate buckling (**b**) (size 2).

The values of the slenderness of the stiffener and the plate determine whether beam–column buckling or local plate buckling plays a major role. To eliminate the influence of stiffener tripping, it is necessary to maintain h_w/t_w and λ_e at a low level.

As shown in Figures 7a and 8a, due to the weak support of the stiffeners provided to the plating, the axial pressure causes stiffened panels to yield at the interface of the plating and stiffener in the mid-span, presenting the deformation simlarly to the initial deformation of beam-column buckling ($m = 1$). The larger the mid-span deflection is, the more significant the effect of beam-column buckling. As shown in Figures 7b and 8b, due to the strong restraint of the stiffeners, the plating first deforms, and the stress distribution is periodic, presenting the deformation as the initial deformation of local plate buckling ($m = 3$). The larger the deflection of the plating between the stiffeners, the more significant the effect of local plate buckling. Through comparison, when the size of the stiffener is increased, the overall stress level of the stiffened panels is increased in the same failure mode.

Current research on the failure modes of stiffened panels is mainly based on the stress and deformation in the limit state. This study believes that the ultimate strength is closely related to the failure mode, and the change trend of the ultimate strength can reflect the failure mode to a certain extent. Figure 9 shows the relationship between the ultimate strength and β for stiffeners of size 2 and the dashed line indicates the critical value of β

for different failure modes. When the failure mode changes from beam–column buckling to local plate buckling, the ultimate strength change trend gradually transforms into an approximate inverse proportional function form.
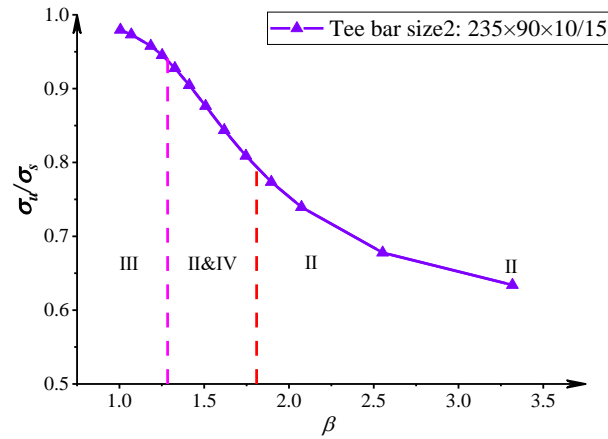

Figure 9. Ultimate strength curve (size 2).

Near the boundary between the beam–column buckling and local plate buckling modes, the equivalent stress of a stiffened panel in the ultimate bearing state is shown in Figure 10. As β increases, the beam–column characteristics ($m = 1$) decrease, the stress gradually presents a periodic distribution, and the buckling deformation of the plate ($m = 3$) increases. $t = 25 \sim 26.5$ mm can be taken as the critical variation range of the failure mode, and the average value can be used as the critical point of the failure mode.
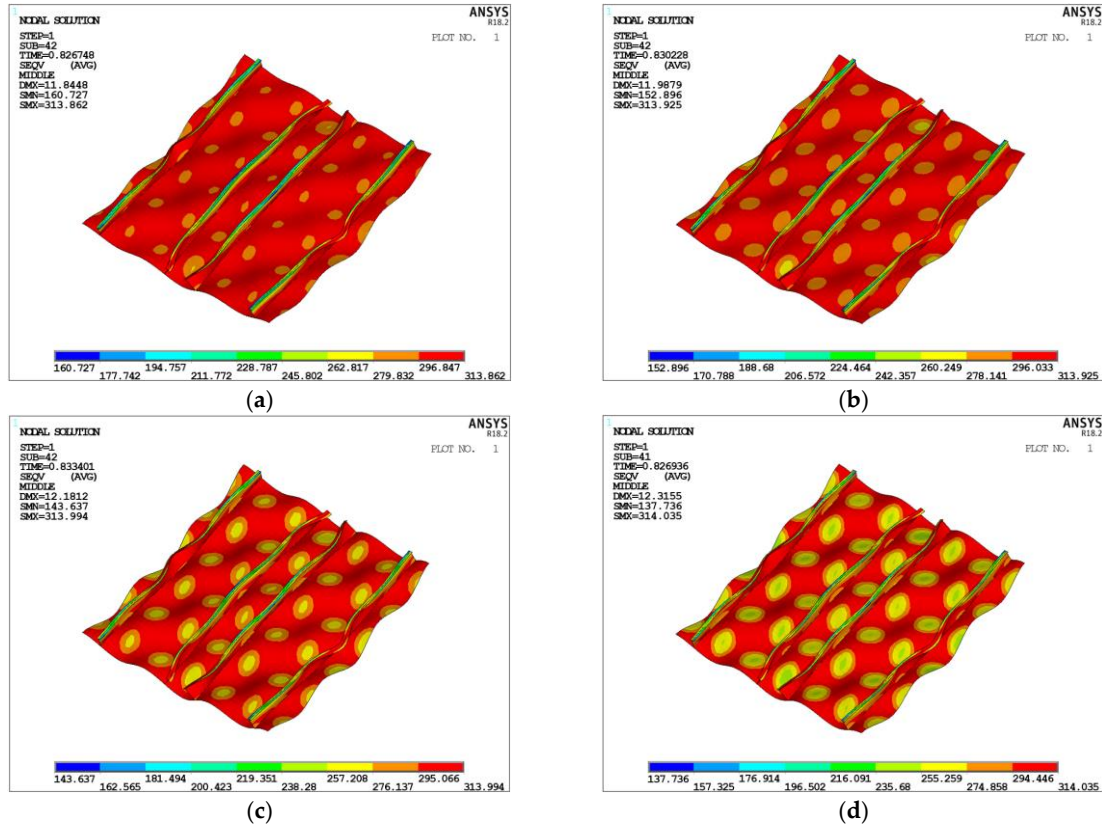

Figure 10. Transition from beam–column buckling to local plate buckling (size 2). (**a**) $t = 28$ mm ($\beta = 1.185$); (**b**) $t = 26.5$ mm ($\beta = 1.252$); (**c**) $t = 25$ mm ($\beta = 1.327$); (**d**) $t = 23.5$ mm ($\beta = 1.412$).

At the same time, the stiffeners show a periodic transverse deformation that is similar to local plate buckling. Since the buckling of a plate at the junction of the plate and stiffeners has an inducing effect on web buckling, plate buckling plays a major role.

3.3. Boundary of Beam–Column Buckling and Local Plate Buckling

To carry out a statistical study on the boundary between beam–column buckling and local plate buckling, a series of stiffener sizes (Table 6) were set that meet the requirements of CSR [15] for the size of T-sections: $h_w/t_w \leq 65\sqrt{k}$, $b_f/t_f \leq 33\sqrt{k}$, $b_f t_f \geq h_w t_w/6$, and material factor $k = 0.78$.

Table 6. Stiffener sizes for the study of local plate buckling and beam–column buckling.

No.	h_w/mm	b_f/mm	t_w/mm	t_f/mm	λ	h_w/t_w	$\lambda_e (t = 22)$
def 1	111.93	56.83	7.3	11	0.812	15.3	0.296
def 2	124.2	71.35	8.1	11.5	0.736	15.3	0.296
size 1	138	90	9	12	0.667	15.3	0.297
def 4	153.33	113.81	10	12.5	0.605	15.3	0.297
def 5	170.2	144	11.1	13	0.550	15.3	0.297
def 6	168.03	44.11	7.15	11.5	0.548	23.5	0.427
def 7	186.83	55.09	7.95	12.5	0.492	23.5	0.427
def 8	207.98	69.1	8.85	13.5	0.442	23.5	0.428
size 2	235	90	10	15	0.391	23.5	0.428
def 10	271.43	121.55	11.55	15.5	0.340	23.5	0.428

To prevent stiffener tripping, h_w/t_w and λ_e (see Section 3.1) were kept at a small level, and the h_w/t_w and λ_e of each dataset were essentially equal. CSR-H [16] specifies that the minimum thickness of hull shell plates is $5.5 + 0.03L_2 \geq 14.5$ mm, and the plating thickness was $t = 13 \sim 33$ mm in this paper.

The ultimate strength of stiffened panels with different combinations of plating and stiffener sizes was calculated. Three factors, the change trend of the ultimate strength, the stress and deformation in the ultimate limit state, were combined to determine the failure mode. The critical points of the failure mode were determined with a certain accuracy (± 0.75 mm), and nonlinear fitting was used to obtain the boundaries of the failure modes, as shown in Figure 11. β and λ have an approximately fourth-order relationship, and β monotonically increases with λ. If the failure mode does not change, the stiffness of the plate and the stiffeners must be maintained at a relatively balanced level.
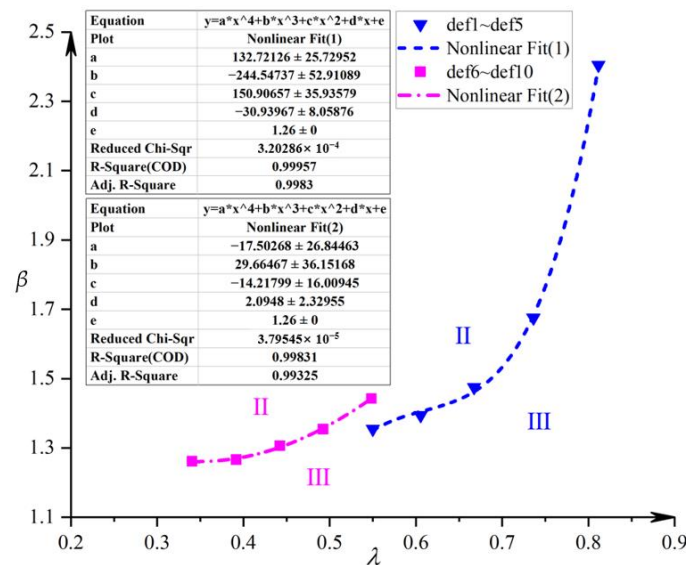

Figure 11. Boundaries of local plate buckling and beam–column buckling.

In addition, an increase in h_w/t_w and λ_e shifts the failure mode boundary to the left, which transforms a part of the area from local plate buckling to beam–column buckling. However, an increase in h_w/t_w and λ_e is conducive to the occurrence of stiffener failure. Various factors must be considered in the reasonable choice of the size of the stiffened panels. Therefore, only a comprehensive analysis of λ, β, h_w/t_w and λ_e can accurately determine the failure mode of a stiffened panel.

4. Study on Stiffener Failure

4.1. Theoretical Formula

The principle of web buckling is similar to the buckling of thin plates. Solving the neutral equilibrium differential equation of a thin plate leads to the ideal elastic buckling critical stress formula:

$$\sigma_E = k\frac{\pi^2 D}{h_w^2 t_w} = k\frac{\pi^2 E}{12(1-\mu^2)(h_w/t_w)^2} \tag{3}$$

where the value of coefficient k is related to b_f/h_w and t_f/t_w [17]. σ_E and h_w/t_w are negatively correlated, and h_w/t_w can be selected as a mechanical parameter for evaluating web buckling.

Stiffener tripping refers to stiffener torsional buckling around the centre of forced rotation. According to the principle of constant potential energy, the ideal elastic buckling critical stress of stiffener tripping can be obtained, which can be written in a similar way to beam–column buckling, as follows:

$$\sigma_E = k\frac{\pi^2 D}{h_w^2 t_w} = k\frac{\pi^2 E}{12(1-\mu^2)(h_w/t_w)^2} \tag{4}$$

where $\lambda_e = [a/(\pi r_e)]\sqrt{\sigma_s/E}$ and r_e is the converted radius of gyration.

A stiffened panel can be regarded as I-beams with different flanges, as shown in Figure 12. With centroid O as the origin, I_1 and I_2 are the moments of inertia of the two flanges to the y-axis. The shear centre S is located on the y-axis, $y_0 = (e_1 I_1 - e_2 I_2)/(I_1 + I_2)$, and the sector moment of inertia is $\Gamma = d^2 I_1 I_2/(I_1 + I_2)$. For a stiffened panel, due to the large difference in the sizes of the plate and the flange of the stiffener, the forced rotation centre C_E is approximately at the intersection of the plate and the centre line of the web; that is, $a_0 \approx dI_2/(I_1 + I_2)$.
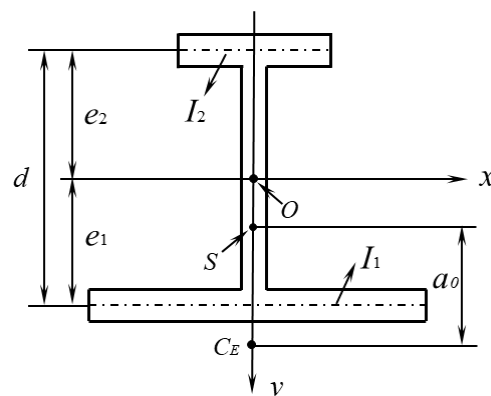

Figure 12. Geometric diagram of the torsion of an I-beam.

The formula [17] for the converted radius of gyration r_e is as follows:

$$r_e^2 = [a^2/(\pi^2 E I_{pc})][GK + 2\sqrt{E(\Gamma + a_0^2 I_y)C}] \tag{5}$$

where $I_{pc} = I_x + I_y + A(a_0 + y_0)^2$ is the polar moment of inertia of the section to C_E. I_x and I_y are the principal moments of inertia of the section to the centroid O. $A = h_f * t_f + h_w * t_w$ is the cross-sectional area of the stiffener. G is the shear modulus. $K = (\sum b_i t_i^3)/3$ is the torsional moment of inertia of the cross-section. $C = Et^3/[3b(1 - \mu^2)]$[18] is the torsional spring stiffness.

Therefore, σ_E and λ_e are negatively correlated, and λ_e can be selected as the mechanical parameter for evaluating stiffener tripping. λ_e is related not only to the stiffener size but also to the plate size.

Notably, since the stiffener web is connected to the plating and stiffener flange, web buckling has a strong coupling effect with local plate buckling and stiffener tripping, respectively. According to the calculations in the IACS standard [16], the web buckling stress is almost always greater than the local plate buckling stress or the stiffener tripping stress in the normal size range. Therefore, stiffener web buckling can be considered to play a secondary role in a stiffened panel with T-section stiffeners. To facilitate the distinction, web buckling is classified into these two failure modes according to the effect of local plate buckling and stiffener tripping, and web buckling is not considered separately. Zhang [8] also adopted a similar approach when classifying the failure modes of stiffened panels.

4.2. Identification of Stiffener Tripping

Figure 13 shows the relationship between the ultimate strength and β for a stiffener of size 3 and the dashed line indicates the critical value of β for different failure modes. When the plate thickness is large, the beam–column overall failure mode is the main form; when the plate thickness is reduced to a certain extent, the beam–column effect is weakened and the tripping effect of the stiffeners is strengthened; when the plate thickness is very thin, local plate buckling plays a major role.
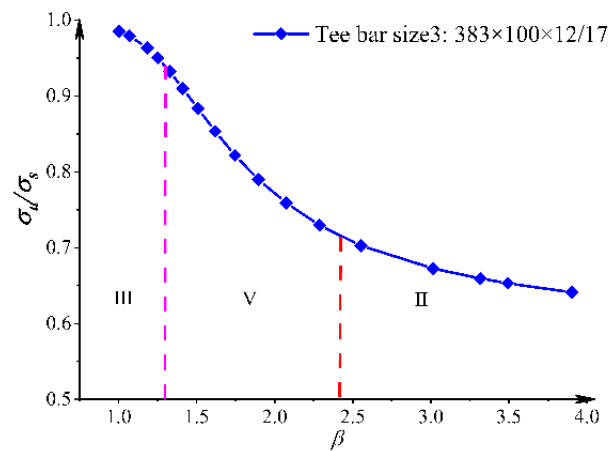

Figure 13. Ultimate strength variation curve (size 3).

As shown in Figure 14, as the plating thickness decreases, the stress level of the stiffeners increases while that of the plating decreases, which means that the characteristics of the beam–column buckling are weakened and stiffener tripping gradually plays a major role. As shown in Figure 15, when the thickness of the plating is 17.5 mm, the stiffener has a high stress and obvious transverse displacement, which is very consistent with the characteristics of stiffener tripping. With the reduction in plating thickness, the stress of the stiffener gradually decreases, and the high-stress region becomes periodic and concentrates at the corners of plating between stiffeners, which means that the failure mode changes from stiffener tripping to local plate buckling.
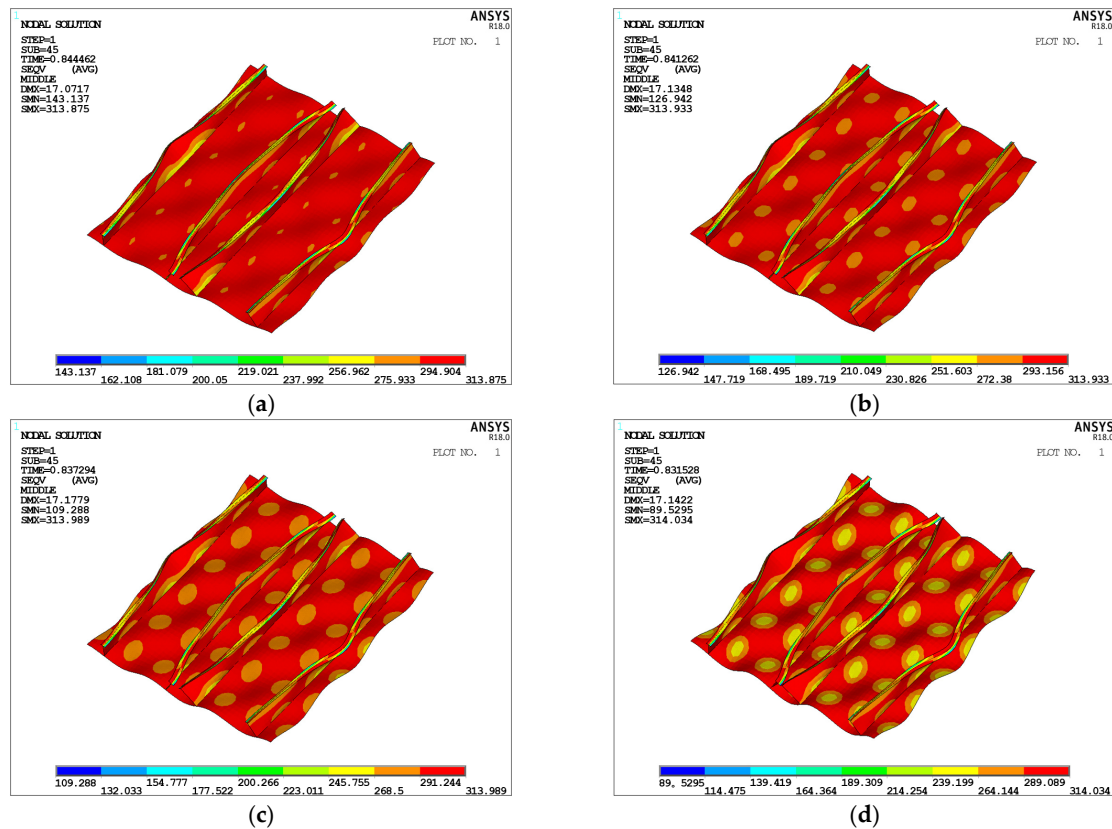
Figure 14. Transition from beam–column buckling to stiffener tripping (size 3). (**a**) $t = 28$ mm ($\beta = 1.185$); (**b**) $t = 26.5$ mm ($\beta = 1.252$); (**c**) $t = 25$ mm ($\beta = 1.327$); (**d**) $t = 23.5$ mm ($\beta = 1.412$).

Combined with the trend of ultimate strength, $t = 25 \sim 26.5$ mm can be regarded as the boundary between beam-column buckling and stiffener tripping, and $t = 14 \sim 16.5$ mm as the boundary between stiffener tripping and local plate buckling.

4.3. Boundaries of Local Plate Buckling, Stiffener Tripping and Beam–Column Buckling

To carry out a statistical study on the boundary of the failure modes of local plate buckling, stiffener tripping, and beam–column buckling, a series of stiffener sizes (Table 7) that meet the CSR requirements was set. The h_w/t_w and λ_e values of each dataset are essentially equal.

The ultimate strengths of stiffened panels with different combinations of plating and stiffener sizes were calculated. Three factors, the trend of the ultimate strength, the stress and deformation in the ultimate limit state, were combined to determine the failure mode and find the boundary of different failure modes. The critical points of the failure mode were determined with a certain accuracy (± 0.75 mm), and nonlinear fitting was used to obtain the boundaries of the failure modes, as shown in Figure 16.

In this study, both h_w/t_w and λ_e were used to evaluate stiffener tripping. It is believed that stiffener tripping only occurs when both h_w/t_w and λ_e are greater than the critical value, and local plate buckling or beam–column buckling only occurs when both h_w/t_w and λ_e are less than the critical value. From λ and β, the coordinates of the critical point $((h_w/t_w)_i, (\lambda_e)_i)$ ($i = 1, 2$) can be determined. If $h_w/t_w > (h_w/t_w)_i \&\& \lambda_e > (\lambda_e)_i$, stiffener tripping occurs; if $h_w/t_w < (h_w/t_w)_i \&\& \lambda_e < (\lambda_e)_i$, local plate buckling or beam–column buckling occurs.
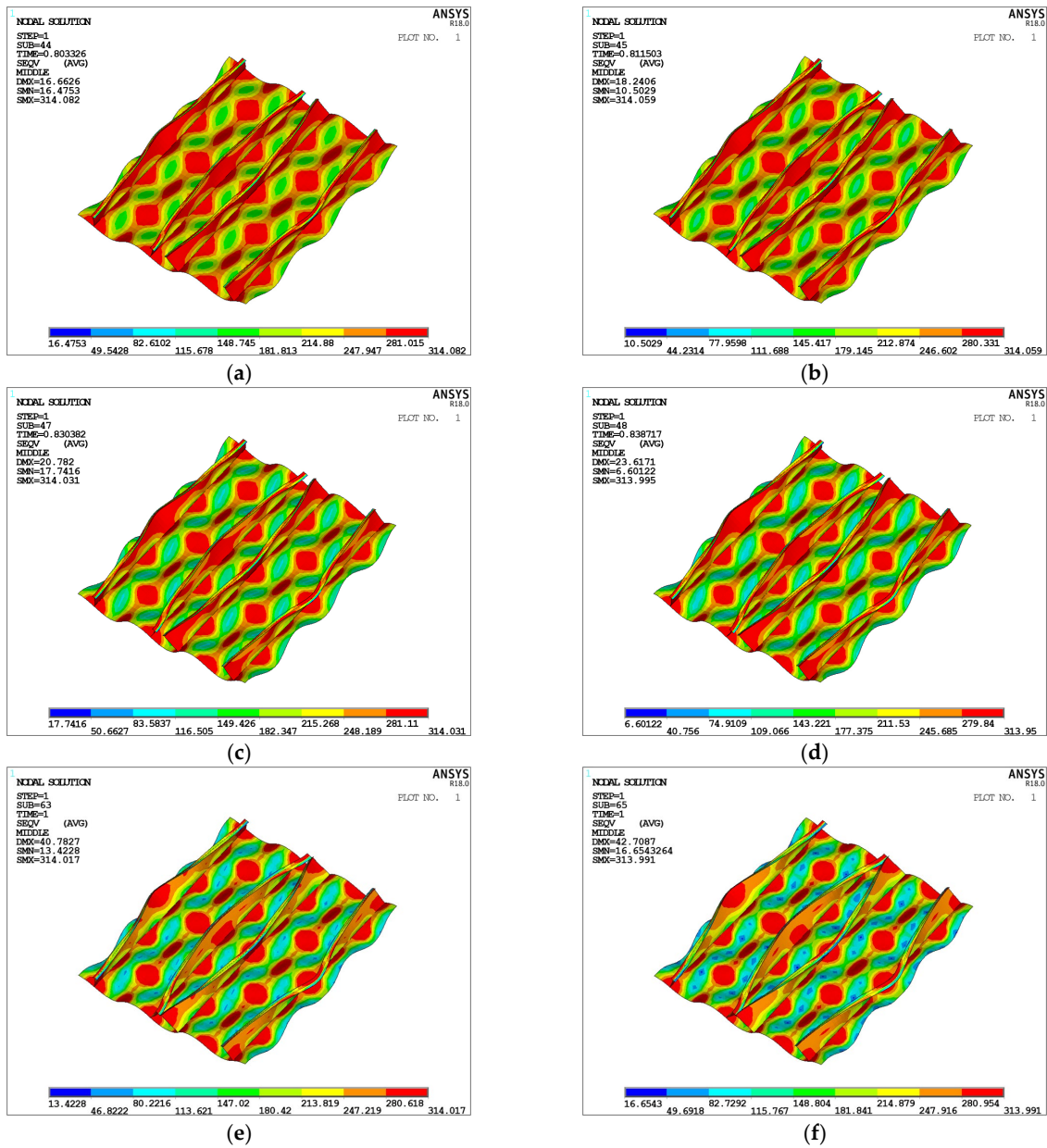
Figure 15. Transition from stiffener tripping to local plate buckling (size 3). (**a**) $t = 17.5$ mm ($\beta = 1.896$); (**b**) $t = 16$ mm ($\beta = 2.074$); (**c**) $t = 14.5$ mm ($\beta = 2.288$); (**d**) $t = 13$ mm ($\beta = 2.552$); (**e**) $t = 11.5$ mm ($\beta = 2.885$); (**f**) $t = 10$ mm ($\beta = 3.318$).

As shown in Figure 17, when λ is constant, $(h_w/t_w)_1$ and $(\lambda_e)_1$ increase with increasing β, which is consistent with the relative relationship between local plate buckling and stiffener tripping. When λ is constant, $(h_w/t_w)_2$ decreases with increasing β, and $(\lambda_e)_2$ does not change much, which is consistent with the relative relationship between stiffener tripping and beam–column buckling. Increasing λ or decreasing h_w/t_w is an effective measure to avoid stiffener tripping.

Table 7. Stiffener sizes for the study of local plate buckling, stiffener tripping and beam–column buckling.

No.	h_w/mm	b_f/mm	t_w/mm	t_f/mm	λ	h_w/t_w	$\lambda_e\,(t = 22)$
case 1	383	92	9.5	15.5	0.244	40.3	0.591
case 2	383	96	10.65	16	0.244	36.0	0.592
size 3	383	100	12	17	0.244	31.9	0.594
case 4	383	103.5	13.5	18	0.244	28.4	0.597
case 5	383	106	15	19	0.244	25.5	0.600
case 6	330	86	8.19	13.5	0.283	40.3	0.531
case 7	330	90	9.18	14	0.283	36.0	0.532
case 8	330	94	10.34	14.5	0.283	31.9	0.533
case 9	330	98	11.63	15	0.283	28.4	0.535
case 10	330	101	12.92	16	0.283	25.5	0.537
case 11	290	82	7.19	12.1	0.321	40.3	0.482
case 12	290	86	8.06	12.5	0.321	36.0	0.482
case 13	290	90	9.09	13	0.331	31.9	0.483
case 14	260	77.5	6.45	11	0.358	40.3	0.447
case 15	260	81	7.23	11	0.358	36.0	0.448
case 16	260	85	8.15	11.5	0.358	31.9	0.448

According to the critical points of the failure modes, the parameters were reasonably selected as dependent variables, and the functional relationships shown in Equations (6)–(8) were obtained through nonlinear fitting.

(6). Critical relationship between Mode II and Mode V:

$$(\lambda_e)_1 = 4.8429\lambda^2 - 3.7355\lambda - 0.0066\beta^2 + 0.3549\beta - 0.3484\lambda\beta + 0.8314$$
$$\lambda = 0.1237\beta^2 - 0.4029\beta + 0.0003\left(\frac{h_w}{t_w}\right)_1^2 + 0.0092\left(\frac{h_w}{t_w}\right)_1 - 0.0101\beta\left(\frac{h_w}{t_w}\right)_1 + 0.3719 \tag{6}$$

(7). Critical relationship between Mode V and Mode III:

$$(\lambda_e)_2 = 3.7232\lambda^2 - 1.6634\lambda + 0.4487\beta^2 - 0.3512\beta - 1.3939\lambda\beta + 0.8683$$
$$\beta = 2.2467\lambda^2 - 1.5263\lambda + 0.0001\left(\frac{h_w}{t_w}\right)_2^2 - 0.0189\left(\frac{h_w}{t_w}\right)_2 + 0.0162\lambda\left(\frac{h_w}{t_w}\right)_2 + 1.8183 \tag{7}$$

(8). Critical relationship between Mode II and Mode III:

$$\beta = 5.5687\lambda^2 - 10.0844\lambda + 13.5317(\lambda_e)_3^2 - 16.7219(\lambda_e)_3 + 15.0091\lambda(\lambda_e)_3 + 6.5261$$
$$\lambda = -0.4530\beta^2 + 1.3132\beta + 0.0005\left(\frac{h_w}{t_w}\right)_3^2 - 0.0849\left(\frac{h_w}{t_w}\right)_3 + 0.0404\beta\left(\frac{h_w}{t_w}\right)_3 - 0.0296 \tag{8}$$

Applicable range: $0.244 \leq \lambda \leq 0.812$, $1.005 \leq \beta \leq 2.552$, $15.333 \leq h_w/t_w \leq 40.316$, and $0.222 \leq \lambda_e \leq 0.852$.

First, λ, β, h_w/t_w and λ_e are calculated from the size of the stiffened panel, and then, λ and β are used as benchmarks to obtain the critical values of $(h_w/t_w)_i$ and $(\lambda_e)_i$ using the functional relationship. The identification method is as follows:

When $(h_w/t_w)_2 < (h_w/t_w)_1 \&\&(\lambda_e)_2 < (\lambda_e)_1$: If $h_w/t_w < (h_w/t_w)_2 \&\&\lambda_e < (\lambda_e)_2$, III is the main failure mode; if $(h_w/t_w)_2 < h_w/t_w < (h_w/t_w)_1 \&\&(\lambda_e)_2 < \lambda_e < (\lambda_e)_1$, II is the main failure mode; and if $h_w/t_w > (h_w/t_w)_1 \&\&\lambda_e > (\lambda_e)_1$, V is the main failure mode.

When $(h_w/t_w)_2 > (h_w/t_w)_1 \&\&(\lambda_e)_2 > (\lambda_e)_1$, V can be ignored: If $h_w/t_w < (h_w/t_w)_3 \&\&\lambda_e < (\lambda_e)_3$, II is the main failure mode; if $h_w/t_w > (h_w/t_w)_3 \&\&\lambda_e > (\lambda_e)_3$, III is the main failure mode.
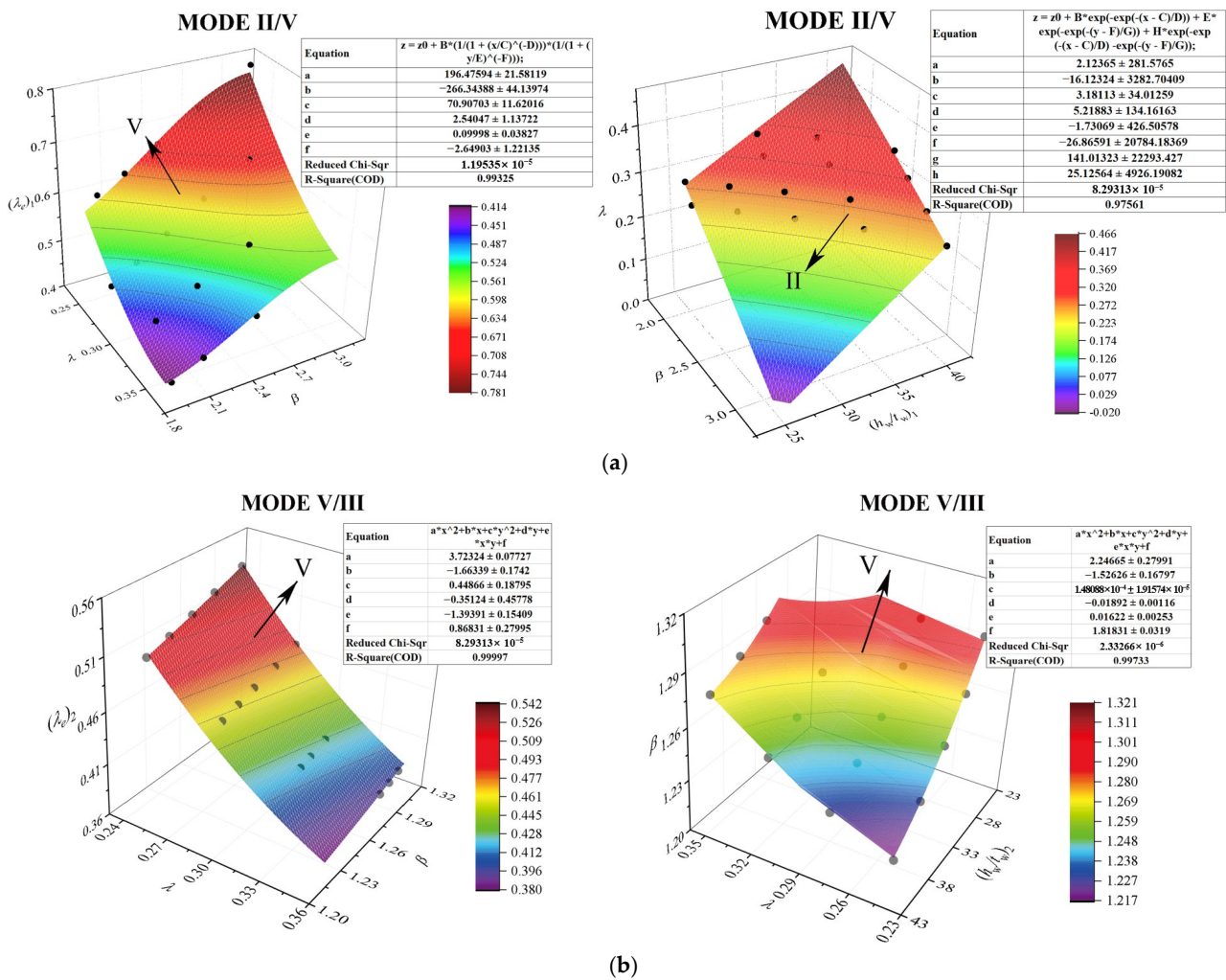
Figure 16. Boundaries of local plate buckling (II), stiffener tripping (V) and beam–column buckling (III). (**a**) Critical surfaces of local plate buckling and stiffener tripping; (**b**) critical surfaces of stiffener tripping and beam–column buckling.
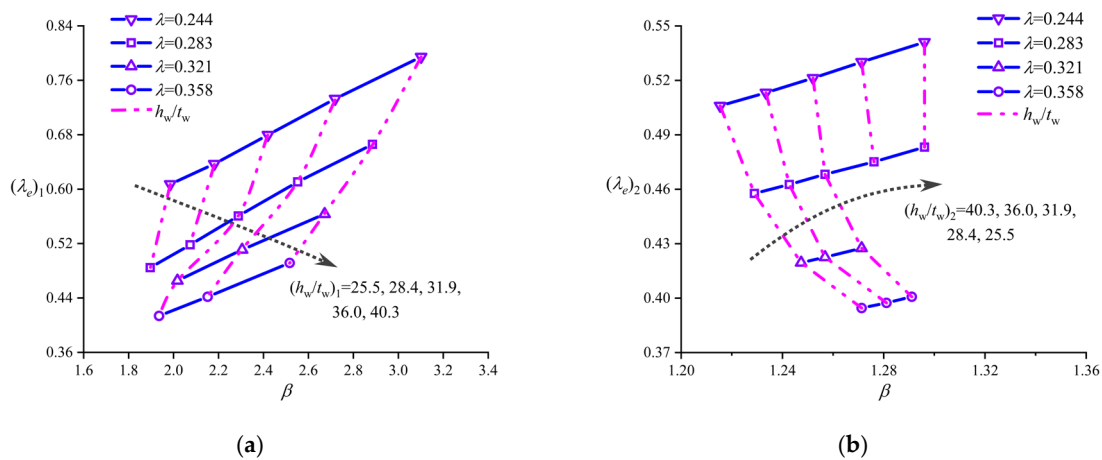
Figure 17. Critical points of local plate buckling (II), stiffener tripping (V) and beam–column buckling (III). (**a**) Critical points of II and V; (**b**) critical points of III and V.

In addition to the above cases, the result can be regarded as a mixed-mode result; that is, there are multiple failure modes, and the effects of these modes on the ultimate strength are similar. At this time, the coupling effect between modes is strong. Additionally, the

margin coefficient *s* can be set to modify the critical values, thereby dividing a certain range near the boundaries into a mixed mode.

Take the stiffened panel with $t = 16$ mm and stiffener of size 2 as an example; the values of $(h_w/t_w)_1$ and $(h_w/t_w)_2$ are 83.68 and 157.90, respectively, which satisfy $(h_w/t_w)_2 > (h_w/t_w)_1$. At the same time, the values of $(\lambda_e)_1$ and $(\lambda_e)_2$ are 0.86 and 0.54, which satisfy $(\lambda_e)_2 > (\lambda_e)_1$. Stiffener tripping does not occur in the ultimate limit state and can be ignored. In this case, since the size of the stiffened panel can also meet the requirement that $h_w/t_w < (h_w/t_w)_3$ and $\lambda_e < (\lambda_e)_3$, the failure mode of can be identified as the local plate buckling (mode II).

The distribution of stress and deformation shown in Figure 18 implies that the failure mode of the stiffened panel is local plate buckling, as predicted, which means that the formula proposed in this paper can realize the prediction of the failure mode.
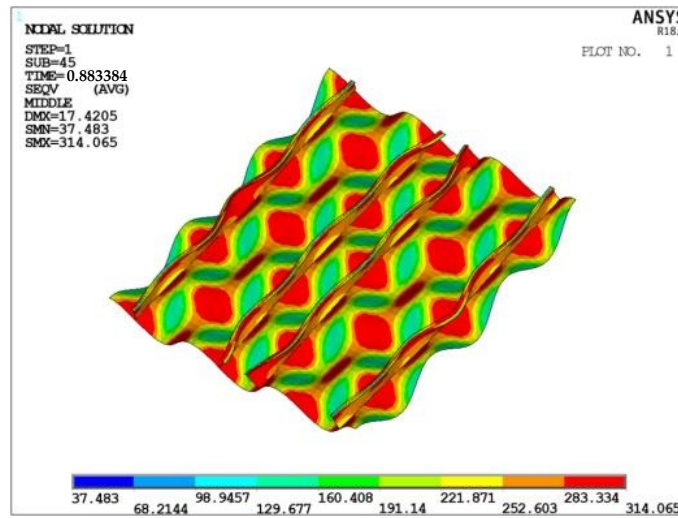

Figure 18. Equivalent stress cloud diagram of stiffened panel ($t = 16$ size 2).

5. Ultimate Strength Evaluation Formula of Stiffened Panels Based on Different Failure Modes

Based on the elastic theory formulas of beam–column buckling, local plate buckling, stiffener web buckling and stiffener tripping and the introduction of a primary term considering plastic range modification, an ultimate strength evaluation in the form of a stiffened panel based on four mechanical parameters is proposed as follows:

$$\frac{\sigma_u}{\sigma_s} = \frac{a_1}{\lambda^2} + \frac{a_2}{\beta^2} + \frac{a_3}{(h_w/t_w)^2} + \frac{a_4}{\lambda_e{}^2} + \frac{b_1}{\lambda} + \frac{b_2}{\beta} + \frac{b_3}{h_w/t_w} + \frac{b_4}{\lambda_e} + c_1\lambda + c_2\beta + c_3 h_w/t_w + c_4\lambda_e + d \tag{9}$$

where σ_u is the ultimate strength of the stiffened panel and $a_1 \sim a_4$, $b_1 \sim b_4$, $c_1 \sim c_4$, and d are undetermined coefficients.

Using MATLAB to perform multivariate function fitting on the ultimate strength of 255 stiffened panels with different failure modes, the calculation formula is as follows:

$$\frac{\sigma_u}{\sigma_s} = \frac{0.0108}{\lambda^2} - \frac{1.0546}{\beta^2} + \frac{222.213}{(h_w/t_w)^2} - \frac{0.0298}{\lambda_e{}^2} - \frac{0.1388}{\lambda} + \frac{2.2403}{\beta} - \frac{23.558}{h_w/t_w} + \frac{0.1796}{\lambda_e}$$
$$- 0.8993\lambda + 0.1302\beta - 0.01058 h_w/t_w + 0.1394\lambda_e + 0.8239 \tag{10}$$

Applicable range: $0.163 \le \lambda \le 0.812$, $1.005 \le \beta \le 3.493$, $15.333 \le h_w/t_w \le 40.316$, and $0.222 \le \lambda_e \le 1.219$.

The coefficient (R^2) of determination of Equation (10) is 0.94708, and the adjusted R^2 is 0.94198. Statistics on the error ((formula value—finite element value)/finite element value) were obtained, as shown in Figure 19. The error of more than 90% of the data is within ±2%, a few results are outside ±4%, the fitting effect is good, and the accuracy of Equation (10) is high.
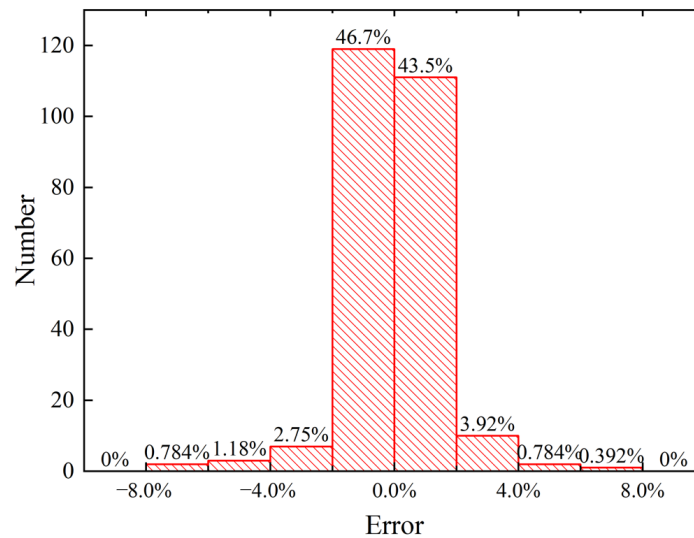

Figure 19. Error frequency distribution histogram.

As shown in Table 8, Equation (10) is compared with the evaluation effect determined by Paik [1] and Zhang [4]. Since the parameters in Paik and Zhang's formulas only contain λ and β, they cannot accurately reflect the effect of stiffener failure. For example, when $t = 22$ or $t = 28$ mm, the ultimate strength is slightly reduced after the stiffener is changed from size 3 to size 4. This is because the effect of increasing h_w/t_w (causing a decrease in the ultimate strength) exceeds the effect of decreasing λ (causing an increase in the ultimate strength).

Table 8. Comparison of the calculation results of the fitting formulas.

t	Sizes of Stiffeners	FEM σ_u/σ_s	Paik	Zhang	Equation (10)	Error of Equation (10)
16	size 1	0.709	0.634	0.722	0.711	0.3%
	size 2	0.740	0.709	0.796	0.751	1.5%
	size 3	0.759	0.739	0.811	0.756	−0.4%
	size 4	0.765	0.751	0.814	0.756	−1.2%
22	size 1	0.807	0.711	0.790	0.813	0.7%
	size 2	0.876	0.793	0.870	0.874	−0.2%
	size 3	0.883	0.827	0.886	0.878	−0.6%
	size 4	0.874	0.840	0.890	0.874	0.0%
28	size 1	0.857	0.755	0.845	0.857	0.0%
	size 2	0.958	0.840	0.931	0.952	−0.6%
	size 3	0.963	0.875	0.948	0.963	0.0%
	size 4	0.946	0.889	0.952	0.958	1.3%

(Note: Zhang): $\sigma_u/\sigma_s = \beta^{-0.28}(1 + \lambda^{3.2})^{-0.5}$; Paik: $\sigma_u/\sigma_s = (0.995 + 0.936\lambda^2 + 0.170\beta^2 + 0.188\lambda^2\beta^2 - 0.067\lambda^4)^{-0.5}$.

6. Conclusions

In this study, through nonlinear finite element analysis, an identification method based on four mechanical parameters is established for common failure modes of stiffened panels, and an ultimate strength evaluation formula suitable for different failure modes is proposed. The conclusions are as follows:

(1) Assuming no stiffener tripping, decreasing λ and increasing h_w/t_w are beneficial to preventing local plate buckling and changing the mode to beam–column buckling. The nonlinear critical curves show that the general form, such as β/λ, struggles to effectively evaluate the failure modes of stiffened panels.

(2) The evolution laws and the relationships of the three failure modes, local plate buckling, stiffener tripping and beam–column buckling, are studied. Increasing λ and decreasing h_w/t_w are beneficial to preventing stiffener tripping. At the same time, the critical function formulas of the three failure modes are fitted for the evaluation of the failure modes.

(3) Based on a large amount of calculation data, a refined formulation of stiffened panels with four parameters is proposed. h_w/t_w and λ_e are added to the formula to reflect the influence of stiffener tripping. The results can provide a reference for the subsequent study of the failure modes of stiffened plates. A comparison with Paik and Zhang shows that the formulation in this paper has a reasonable form and good precision.

However, it may be too ideal to determine the failure mode by considering the variation trend of the ultimate strength and stress distribution in the ultimate limit state. In subsequent work, more accurate methods for determining failure modes need to be developed, which could improve the accuracy of critical function formulas and ultimate strength.

Author Contributions: Conceptualization, Q.Z.; Methodology, H.Y.; Software, H.Y. and W.C.; Validation, S.W. and W.C.; Resources, Y.H.; Data curation, S.W.; Writing—original draft, H.Y.; Writing—review & editing, H.Y. and S.W.; Supervision, Q.Z. and Y.L.; Project administration, Q.Z. and Y.L.; Funding acquisition, Y.H. All authors have read and agreed to the published version of the manuscript.

Conflicts of Interest: The authors declare no conflict of interest.

Nomenclatures

λ	Column slenderness
β	Plate slenderness
h_w/t_w	Height-to-thickness ratio of stiffener
λ_e	Stiffener tripping slenderness
σ_s	Yield stress
σ_u	Ultimate strength of stiffened panels
I	Moment of inertia of the section
σ_E	Elastic buckling stress
I_1, I_2	Moments of inertia of the two flanges to the y-axis
Γ	Sector moment of inertia
C_E	Forced rotation centre
I_{pc}	Polar moment of inertia of the section
I_x, I_y	Principal moments of inertia of the section to the centroid
G	Shear modulus
K	Torsional moment of inertia of the cross-section
C	Torsional spring stiffness

References

1. Paik, J.K.; Thayamballi, A.K. An empirical formulation for predicting the ultimate compressive strength of stiffened panels. In Proceedings of the 7th International Offshore and Polar Engineering Conference, Honolulu, HI, USA, 25–30 May 1997.
2. Paik, J.K. Empirical formulations for predicting the ultimate compressive strength of welded aluminum stiffened panels. *Thin-Walled Struct.* **2007**, *45*, 171–184. [CrossRef]
3. Khedmati, M.R.; Zareei, M.R.; Rigo, P. Empirical formulations for estimation of ultimate strength of continuous stiffened aluminium plates under combined in-plane compression and lateral pressure. *Steel Constr.* **2010**, *48*, 274–289. [CrossRef]
4. Zhang, S.; Khan, I. Buckling and ultimate capability of panels and stiffened panels in axial compression. *Mar. Struct.* **2009**, *22*, 791–808. [CrossRef]
5. Faulkner, D.; Adamchak, J.C.; Snyder, G.J.; Vetter, M.F. Synthesis of welded grillages to withstand compression and normal loads. *Comput. Struct.* **1973**, *3*, 221–246. [CrossRef]
6. Xu, M.C.; Song, Z.J.; Zhang, B.W.; Pan, J. Empirical formula for predicting ultimate strength of stiffened panel of ship structure under combined longitudinal compression and lateral loads. *Ocean Eng.* **2018**, *162*, 161–175. [CrossRef]
7. Grondin, G.Y.; Elwi, A.E.; Cheng, J.J.R. Buckling of stiffened steel plates—A parametric study. *J. Constr. Steel Res.* **1999**, *50*, P151–P175. [CrossRef]
8. Ozguc, O. Nonlinear Buckling Simulations of Stiffened Panel Exposed to Combination of Transverse Compression, Shear Force and Lateral Pressure Loadings. *J. Inst. Eng. India Ser. C* **2021**, *102*, 397–408. [CrossRef]
9. Ringsberg, J.W.; Darie, I.; Nahshon, K.; Shilling, G.; Vaz, M.A.; Benson, S.; Yanagihara, D. The ISSC 2022 committee III. 1-Ultimate strength benchmark study on the ultimate limit state analysis of a stiffened plate structure subjected to uniaxial compressive loads. *Mar. Struct.* **2021**, *79*, 103026. [CrossRef]
10. Paik, J.K.; Kim, B.J. Ultimate strength formulations for stiffened panels under combined axial load, in-plane bending and lateral pressure: A benchmark study. *Thin-Walled Struct.* **2002**, *40*, 45–83. [CrossRef]
11. Paik, J.K.; Amlashi, H.; Boon, B.; Branner, K.; Caridis, P.; Das, P.; Yang, P. ISSC2012–Committee III.1 Ultimate Strength. In Proceedings of the 18th International Ship and Offshore Structures Congress (ISSC). Rostock, Germany, 10–13 September 2012; Volume 1.
12. Xu, M.C.; Yanagihara, D.; Fujikubo, M.; Soares, C.G. Influence of boundary conditions on the collapse behaviour of stiffened panels under combined loads. *Mar. Struct.* **2013**, *34*, 205–225. [CrossRef]
13. Frieze, P.A.; Abbattista, M.; Vallascas, M.; Paik, J.K. A Benchmark Study of ISO 18072-2 on the Stiffened Panel Ultimate Strength. In Proceedings of the ASME 2011 30th International Conference on Ocean, Offshore and Arctic Engineering, Rotterdam, The Netherlands, 19–24 June 2011.
14. Von Karman. *Die Millragenc Bricite*; Springer: Berlin, Germany, 1924.
15. Class, N.K. Rules for the survey and construction of steel ships. *Part CSR-B Common Struct. Rules Bulk Carr.* **2015**, *2015*, 406–408.
16. IASC. *Common Structural Rules for Bulk Carriers and Oil Tankers*; International Association of Classification Societies: London, UK, 2019.
17. Bleich, F. *Buckling Strength of Metal Structures*; McGraw-Hill Book Co.: New York, NY, USA, 1952.
18. Hu, Y.; Chen, B.; Sun, J. Tripping of thin-walled stiffeners in the axially compressed stiffened panel with lateral pressure. *J. Shanghai Jiaotong Univ.* **2000**, *37*, 1–26. [CrossRef]